HHS Public Access

Author manuscript

IEEE Trans Biomed Eng. Author manuscript; available in PMC 2018 May 01.

Published in final edited form as:

IEEE Trans Biomed Eng. 2017 May ; 64(5): 1003–1010. doi:10.1109/TBME.2016.2585109.

Simultaneous Monitoring of Ballistocardiogram and Photoplethysmogram Using Camera

Dangdang Shao[1], **Francis Tsow**[1], **Chenbin Liu**[2], **Yuting Yang**[2], and **Nongjian Tao**[1,2,*]

[1]Center for Bioelectronics and Biosensors, Biodesign Institute, Arizona State University, Tempe, AZ 85281, USA

[2]School of Chemistry & Chemical Engineering, Nanjing University, Nanjing, Jiangsu 210093, China

[1,2]Center for Bioelectronics and Biosensors, Biodesign Institute, Arizona State University, Tempe, AZ 85281, USA, and School of Chemistry & Chemical Engineering, Nanjing University, Nanjing, Jiangsu 210093, China

Abstract

We present a noncontact method to measure Ballistocardiogram (BCG) and Photoplethysmogram (PPG) simultaneously using a single camera. The method tracks the motion of facial features to determine displacement BCG, and extracts the corresponding velocity and acceleration BCGs by taking first and second temporal derivatives from the displacement BCG, respectively. The measured BCG waveforms are consistent with those reported in literature and also with those recorded with an accelerometer-based reference method. The method also tracks PPG based on the reflected light from the same facial region, which makes it possible to track both BCG and PPG with the same optics. We verify the robustness and reproducibility of the noncontact method with a small pilot study with 23 subjects. The presented method is the first demonstration of simultaneous BCG and PPG monitoring without wearing any extra equipment or marker by the subject.

Index Terms

ballistocardiogram; photoplethysmogram; remote sensing

I. Introduction

BCG measures repetitive body motion caused by the cardiac contraction and ejection of blood during cardiac cycles. BCG waveform contains features that can indicate some physiological attributes [1, 2], and an irregular BCG may reveal abnormal circulation and cardiac diseases [3–6]. Typically, a BCG waveform consists of several waves, which are distinguished by shape, relative amplitude, and the sequence of occurrence. Each of these constituents is associated with a different cardiac event [7]. For instance, the “IJ wave” of acceleration BCG may be used to measure ejection force and stroke volume [8–12]. An

*correspondence: njtao@asu.edu.

increase in IJ amplitude implies an increase in cardiac ejection, which can be used as a potential indicator of recovery in patients with heart diseases.

Starr introduced modern BCG in 1930s [1–3, 6, 11–14]. Traditionally, BCG measurements used table-based apparatuses, such as suspended bed [13], and suspended rigid platform [15]. Elliott et al. developed an electrochemical method to measure BCG [16]. These BCG apparatuses were bulky and hard to implement compared with other medical procedures, such as electrocardiography (ECG), which led to a decline in the use of BCG after 1970s. With the development of new sensor technologies, BCG has attracted research interest again in recent years. An ear-worn device was demonstrated for ECG, BCG, and PPG monitoring [9, 17–19], where the BCG was obtained from an accelerometer integrated in the device. Other approaches used to measure BCG include weighing scale [8, 20–23], polypropylene film coated with electrically conductive layers [24, 25], and force sensor mounted in bed [26]. In addition to these acceleration and force measurements, displacement BCG was also obtained using a linear variable displacement transformer position sensor [27].

The aforementioned BCG monitoring methods require direct contact between the measuring instrument and subject, which is not always desirable. A noncontact video-based method can provide a more natural and comfortable way for BCG monitoring. Moreover, it is an MRI-safe measurement that can track the subject's cardiac activities in a changing magnetic field environment [28]. However, noncontact monitoring of BCG is not well established. Balakrishnan et al. [29] detected heart rate by tracking the vertical movement of head, but the full BCG features were not resolved. Krug et al. [28] used a camera to track the motion of a marker with moiré pattern worn by the subject on the nasal bridge. The subject also needed to wear a head coil fitted with a cushion to avoid motion artifacts.

PPG tracks the blood volume change caused by cardiac activity. Single-wavelength PPG can be used to monitor heart rate, heart rate variability (HRV) and respiration rate [30–32]. Dual-wavelength PPGs can be used to measure blood oxygen saturation [33, 34]. Two PPGs, or one PPG with another cardiac signal (ECG or BCG) can further provide pulse transit time [35–37]. Traditional PPG measurements are based on contact methods. Recently, noncontact PPG measurement by using camera has been demonstrated by several groups [30, 33, 38], including us [35].

In this paper, we report a noncontact method to monitor BCG and PPG simultaneously at the same body location using a single camera. To the best of authors' knowledge, this is the first demonstration of simultaneous BCG and PPG monitoring without wearing any extra equipment or marker by the subject. The BCG measured using the presented noncontact method showed a similar waveform as that measured using direct body BCG system [14]. Furthermore, we validated the method by comparing the BCGs with those recorded with an accelerometer worn by the subjects.

II. Methods

A. Data acquisition

A Pike color camera (F-032C) was used to capture the video of a subject's face at a frame rate of 60 frames/second under indoor ambient light condition (Fig. 1(a)). BCG acquisition is easily affected by various noise factors, such as respiratory activity and random body movement [1]. To minimize the latter, the subject was asked to lie down, face upward, on a yoga mat at a distance of approximately 0.5 m from the camera lens. Based on current experiment setting, one pixel in the captured image is equivalent to approximately 1×10^{-4} m on the subject's face. The video was recorded for 30 seconds in each experiment. The first 10 seconds of the video are discarded during processing, since that is the amount of time it takes the camera to ramp up to the desired stable frame rate of 60 frames/second. BCG and PPG were determined from the video with different algorithms as described below (Fig. 1(b)).

For BCG detection, we selected a region of interest (ROI), including at least one facial feature. For each subject, based on his or her personal characteristics, we found multiple options of the facial feature that could be used to track BCG. Examples of the features that we have successfully used include mole, facial hair, nostril, acne, and skin pigmentation. The BCGs from different facial features on the same subject were similar (Fig. 3).

Mouth, and its surrounding area, was selected as the ROI due to the availability of abundant distinct facial features for BCG tracking (Fig. 1(c)). The PPG signal obtained from this ROI was also satisfactory.

B. Signal Processing

Feature points in the defined ROI were detected from the first frame of the video based on the method proposed by Shi et al. [39]. The motion of each detected feature point was tracked over video frames with the Kanade-Lucas-Tomasi algorithm (KLT) [40, 41]. For an affine motion field

$$\delta = Dx + d, \quad (1)$$

where d is the translation of the feature window's center and D is the deformation matrix, which is given by

$$D = \begin{bmatrix} d_{xx} & d_{xy} \\ d_{yx} & d_{yy} \end{bmatrix}. \quad (2)$$

KLT determines the motion parameters D and d that minimize the dissimilarity ε between two adjacent frames, viz. I and J, in a given feature window around position x. ε is expressed as

$$\varepsilon=\int\int_{W}\{J[(1+D)x+d]-I(x)\}^2 w(x)dx, \quad (3)$$

where $w(x)$ is the weighting function.

The vertical displacement (in the direction along feet to head) contains BCG [17, 28], which was analyzed in detail. To convert the feature dimensions represented in terms of the number of pixels into meters, we defined a conversion factor as

$$\alpha=\frac{\text{feature\_ dimension}(m)}{\text{feature\_ pixel\_ number}(pixel)}. \quad (4)$$

This conversion factor was determined by measuring facial feature dimension (e.g., mouth) using a ruler and counting the pixel numbers of the corresponding feature in the image.

For each frame, n, the vertical components of point locations, y_i, were averaged over all the detected feature points, and plotted against time to provide displacement BCG_d, which can be written as

$$BCG_d(n)=\frac{\sum_{i=1}^{k} y_i(n)}{k}\times\alpha, \quad (5)$$

where k is the number of detected feature points and may vary depending on the type of facial feature.

The first and second temporal derivatives of the displacement BCG were then calculated, leading to velocity BCG_v and acceleration BCG_a, respectively.

We used a method introduced in [31] to calculate PPG, whereby the image intensity of green and red channels, I_g and I_r, were averaged over all the ROI pixels in every frame, and then normalized by the corresponding averages, $\mu(I_g)$ and $\mu(I_r)$, over a time interval,

$$PPG(n)=\frac{I_g(n)/\mu(I_g)}{I_r(n)/\mu(I_r)}-1. \quad (6)$$

This method is less affected by motion compared to the method when a single color channel (e.g., green) is used [31].

C. PPG evaluation

Signal-to-noise ratio (SNR) was analyzed for the measured PPG using a similar method as [31] and [42]. We computed a 1200-point FFT and detected the heart rate using peak detection in the frequency domain. The majority of PPG power is found around heart rate (~ 1 Hz) and its corresponding harmonics. The signal power was then defined as the sum of the squared magnitudes of 5 bins around the heart rate, and 5 bins each around the second and third harmonics. The noise power was the sum of the squared magnitudes of all the other bins in the pulse frequency range (0.5 – 4 Hz). The ratio of signal power to noise power provided SNR according to

$$SNR=10\log_{10}\left(\frac{\sum_{f=0.5}^{4}\left(U_t(f)S(f)\right)^2}{\sum_{f=0.5}^{4}\left(1-U_t(f)\right)S(f)^2}\right) \quad (7)$$

where $S(f)$ is the spectrum of the signal, f is the frequency (Hz), and $U_t(f)$ is a binary window to pass the pulse frequency and isolate the noise frequency.

D. BCG feature extraction and evaluation

We extracted several features from measured BCG waveforms, including ensemble averages, IJ intervals and amplitudes. Ensemble averaging was performed over the obtained waveforms to look into the morphology of these signals. In order to obtain the ensemble average, we plotted the 20 seconds duration signal as an eye diagram over one cardiac cycle. Multiple individual cycles (~ 20 beats) were aligned and then averaged to obtain an ensemble waveform. This is similar to the methods reported in literature [19, 20] to analyze BCG. A time duration of 20 seconds results in adequately stable ensemble waveform [19]. IJ interval was calculated as the time difference between acceleration BCG I_a peak and J_a peak in the same beat, while IJ amplitude was the absolute value of the amplitude from I_a peak to J_a peak.

Compared to PPG, BCG frequency components are more complex and have a wider distribution in the spectrum (Fig. 2(e, f)). The majority of BCG power stays in the range of 1 – 10 Hz [19, 24]. Therefore, we evaluated the SNR of BCG based on two methods: one of them employing maximum likelihood and the other using sample correlation coefficient [20, 43].

SNR estimation based on maximum likelihood can be obtained by:

$$SNR_{ML}=\frac{2\sum_{i=1}^{N}EA_{sub,1}(i)EA_{sub,2}(i)}{\sum_{i=1}^{N}(EA_{sub,1}(i)-EA_{sub,2}(i))^2}, \quad (8)$$

where $EA_{sub,1}$ is the sub-ensemble average for the first 10 seconds of the measured displacement BCG, and $EA_{sub,2}$ is that for the remaining 10 seconds. N is the number of samples in the sub-ensemble averages, and i is the sample time index.

Another SNR estimation method is based on sample correlation coefficient r:

$$r=\frac{\sum_{i=1}^{N}EA_{sub,1}(i)EA_{sub,2}(i)}{\sqrt{\sum_{i=1}^{N}EA_{sub,1}(i)^2\sum_{i=1}^{N}EA_{sub,2}(i)^2}}. \quad (9)$$

The SNR can be then calculated as:

$$SNR_r=A\frac{r}{1-r}+B, \quad (10)$$

where A and B are given by:

$$A=\exp(\frac{-2}{N-3}), \quad (11)$$

$$B=-\frac{1}{2}(1-\exp(\frac{-2}{N-3})). \quad (12)$$

E. Reference technology

We have validated PPG detection in our previous work [35]. To validate the presented BCG detection method, we compared the measured BCG waveforms against those in literature [14, 44], and also carried out BCG measurement simultaneously with the accelerometer, which is a well-accepted method for acceleration BCG monitoring [9, 17, 18, 45]. The accelerometer (LSM330) used for the purpose of this study is that found in a commercial off-the-shelf Samsung S4 smartphone. The sample rate of the accelerometer is set at 50 Hz, and based on the datasheet [46], the linear acceleration sensitivity is typically around 0.007 m/s^2. The noise level is about 0.005 m/s^2, which is estimated from the standard deviation by keeping the smartphone stationary on a flat surface for 30 seconds. For measurements with

test subjects, the smartphone was placed on the subject's forehead and held in place with a rubber band (Fig. 1(a)). The y-axis (feet-head direction) acceleration measured by the accelerometer was compared to the vertical acceleration BCG obtained using the presented method. The Pearson's linear correlation coefficients between ensemble averages, IJ amplitudes and intervals obtained using the two methods were calculated.

F. Pilot study participant information

We carried out a small-scale pilot study to demonstrate the presented video-based method for monitoring BCG and PPG simultaneously. The study included 23 subjects (approved by Institutional Review Board at Arizona State University, No. STUDY00003483). The subjects included 15 males and 8 females of different ages (29 ± 5 years old, mean ± SD) and ethnic profiles, and from different regions (North America, South America, East Asia and South India). The skin colors of the subjects ranged from type II (white) to type V (brown) based on the Fitzpatrick scale [47]. Informed consents were obtained from all the subjects following an approved protocol. None of the subjects had any known cardiovascular disease.

III. Results

A. BCG and PPG

We obtained the displacement BCG and PPG simultaneously from a video of each subject. Fig. 2 shows the results for a male subject. The J_d-peak, one of the most prominent features of BCG, is clearly resolved in the displacement BCG obtained with the presented video method (Fig. 2(a)). The corresponding velocity and acceleration BCGs were obtained by taking first and second temporal derivatives, and then filtering them with a 2^{nd} order Butterworth filter with a passband of [0.5, 10] Hz (Fig. 2(b) and Fig. 2(c)). The obtained PPG is shown in Fig. 2(d). DC bias is removed from these signals. Ensemble averages of these waveforms are provided on the right of the figures. The power spectra of the displacement BCG and PPG are shown in Fig. 2(e, f).

Fig. 3 shows the BCGs detected from three different facial features (facial hair, mole and nostril) using the same video of a male subject. BCGs obtained from different features look very similar. The Pearson's linear correlation coefficients between every two signals are larger than 0.95, implying that the displacement BCGs obtained from the three features are strongly correlated.

B. Validation of BCG detection

To validate the presented video-based noncontact method for BCG detection, we carried out simultaneous measurement of BCG with a reference device (accelerometer). The acceleration BCGs along feet-head direction obtained using the presented, and the reference methods are plotted in Fig. 4. Both waveforms are filtered with a 2^{nd} order Butterworth filter with a passband of [0.5, 10] Hz. The obtained BCG waveform from the video is resampled from 60 Hz to 50 Hz to match the sampling rate of the accelerometer for comparison purpose. The overall patterns and the obtained cardiac cycles from the two methods are

consistent with each other, which validates the presented noncontact method for BCG monitoring.

To further examine the detailed features of the BCGs obtained with the two methods, ensemble averaging was performed for two subjects over a duration of 20 seconds, and the resulting waveforms, including individual cycles (dash lines) and ensemble averages (solid lines), are shown in Fig. 5.

For both subjects, the major peaks in BCG waveforms from the presented and reference methods are similar, and the Pearson's linear correlation coefficients are larger than 0.95, implying that the test results obtained from the two methods are strongly related. Furthermore, the obtained BCGs from both methods are also consistent with the typical direct body measurement BCG waveforms reported in literature [14, 45].

C. Small-scale pilot study

In the small-scale pilot study, we performed the test as described in previous section on each subject. Fig. 6 shows the displacement BCGs obtained from seven different subjects for the purpose of demonstration. The overall BCG waveforms are similar for all subjects, but the detailed features show substantial variations due to different physiological attributes, which have also been reported by other literatures [20, 48, 49]. The largest amplitudes of the measured displacement BCG J-peaks ranged from 1×10^{-4} to 2×10^{-4} m. The velocity and acceleration peaks varied from 2×10^{-3} to 6×10^{-3} m/s, and 0.05 to 0.15 m/s^2, respectively. These values are comparable to those reported by other researchers using different methods (Table I). For the same subject, the measurement error for these values was about 10% in consecutive tests.

We compared the IJ amplitudes (|a|) and intervals (t) of acceleration BCGs determined using the presented method with those using the reference accelerometer. Figs. 7 and 8 show the plots of these two values from 73 tests with linear least square regression. Good linear correlation is found between the presented and reference methods for both plots ($R^2 = 0.82$ and $R^2 = 0.7$). The difference between the two methods may be attributed to different body locations (mouth region for presented method and forehead for accelerometer). The accuracy may also be affected by the calibration error.

Fig. 9 summarizes the Pearson's linear correlation coefficients between the BCGs measured using the presented method and reference accelerometer. Fig. 10 shows the BCG SNR values based on maximum likelihood (8) and sample correlation coefficient (10) using the presented method. All the test results are divided into four groups based on the types of facial features used for motion tracking. The SNR values and the standard deviations are comparable to those in [20] using weighing scale. Fig. 9 and Fig. 10 suggest that the selection of facial features is not a key factor for video-based BCG monitoring since the values are comparable among different features.

To evaluate PPG quality, we plotted the PPG SNR, as shown in Fig. 11. All the test results are divided into four different skin types. The overall SNR values are comparable to other

studies [31, 42]. The SNR values from lighter skin tone subjects are better than darker skin tone subjects, which have also been reported by other researchers [31].

D. Signals from other posture

We also validated the presented method against sitting position. Fig. 12. shows the signals obtained when the subject was sitting on a chair. BCG was obtained by tracking facial feature (mole) and PPG was obtained from the mouth region, using the same methods as described in the previous section. The subject was the same as the one in Fig. 2. Accelerometer was also used as reference device for comparison. The Pearson's linear correlation coefficient between the presented method (Fig. 12(c)) and reference device (Fig. 12(e)) is 0.97. BCG waveforms show difference between sitting and supine positions, which has also been reported in other literature [25].

IV. Discussion

We presented a noncontact method to monitor BCG and PPG simultaneously from the same video. The selection of facial features is not critical for BCG monitoring, but sharp focus of facial features in the video is beneficial for accurate tracking of BCG. SNRs of PPG from dark skin subjects were slightly worse than that from light skin subjects, but the overall quality is satisfactory for all the cases. However, the presented method will face challenge in the extreme case when the subject face is covered with heavy make-up, or no sharp features, such as nose or mouth, are recorded in the video, which will make it difficult for our proposed method to perform intensity analysis or track motion for PPG and BCG measurements. We validated the presented method with both supine and sitting positions. Compared to supine position, sitting position is more easily affected by motion artifacts, since the body is more prone to involuntary movement in the latter posture due to an absence of support that is typically afforded in the former posture.

Future works will include improvement of the BCG and PPG qualities via different approaches. Firstly, the temporal resolutions of BCG and PPG are constrained by video frame rate, which is currently 60 frames/second. A faster camera could be used to improve the temporal resolution, which will be beneficial for analyzing the high frequency features and the timing characteristics of the signals. Secondly, since both BCG and PPG are sensitive to motion-induced artifacts, effective tracking algorithms may help to mitigate noise due to unrelated body motions. Thirdly, BCG may affect PPG [51]. Taking difference between two normalized color channels may help make PPG less affected by motions (including BCG), as in (6). Implementation of more advanced chrominance-based methods may further help minimize the artifacts [31]. Accurate measurements of BCG and PPG may help better interpretation of these waveforms for further applications.

Future works will also include clinical studies with more subjects, especially those with abnormal cardiovascular functions, which will help relate BCG features to physiological conditions of the subjects, and further validate the clinical value of the presented technique. Finally, pulse transient time (PTT) could be obtained from BCG and PPG, from which, one may estimate blood pressure without using a cuff [18, 52, 53].

V. Conclusion

The presented work is the first demonstration of simultaneous noncontact BCG and PPG monitoring without wearing any extra equipment or marker by the subject. From the displacement BCG, velocity and acceleration BCGs are obtained. The acceleration BCG waveforms were consistent with those reported in the literature, and were validated with an accelerometer-based reference method. We verified the robustness and reproducibility of our method with a small-scale pilot study involving 23 subjects with different ethnic profiles and skin tones (light and dark skin colors).

The presented method shows that in addition to PPG, BCG can also be obtained from the same body location, which potentially provides a low-cost solution to record physiological parameters related with these two signals simultaneously using a single camera under normal living conditions. PPG contains key information about heart rate, heart rate variability, and saturated blood oxygen level. The addition of BCG provides more cardiovascular parameters (e.g., stroke volume). With both BCG and PPG, blood pressure may be determined.

Acknowledgments

This work was supported by the National Natural Science Foundation of China (NSFC, Grant No. 21327902).

The authors would like to thank Rafael Iriya for discussions.

References

1. Starr I. On reading ballistocardiograms. Am J Cardiol. Oct; 1958 2(4):404–416. [PubMed: 13582883]
2. Starr I. Essay on the ballistocardiogram. J AM Med Assoc. Aug; 1954 155(16):1413–1425. [PubMed: 13183760]
3. Starr I, et al. Ballistocardiogram. II. Normal standards, abnormalities commonly found in diseases of the heart and circulation, and their significance. J Clin Invest. May; 1940 19(3):437–450. [PubMed: 16694759]
4. Jackson DH, et al. Ballistocardiographic and angiographic correlation study in idiopathic hypertrophic subaortic stenosis. Bibl Cardiol. Jan.1971 27:14–20.
5. Goedhard W. Ballistocardiography: past, present and future. Bibl Cardiol. 1978; 37:27–45.
6. Starr I, et al. Twenty-year studies with the Ballistocardiograph. Circulation. May; 1961 23(5):714–732.
7. Thompson WB, et al. Ballistocardiography. II. The normal ballistocardiogram. Circulation. Mar; 1953 7(3):321–328. [PubMed: 13033059]
8. Giovangrandi, L., et al. Ballistocardiography—a method worth revisiting. Proc. IEEE Eng. Med. Biol. Soc; Boston, Massachusetts, USA. 2011; p. 4279-4282.
9. He D, et al. An ear-worn vital signs monitor. IEEE Trans Biomed Eng. Oct; 2015 62(11):2547–2552. [PubMed: 26208264]
10. van Brummelen AGW, et al. On the elimination of pulse wave velocity in stroke volume determination from the ultralow-frequency displacement ballistocardiogram. Am Heart J. Mar; 1964 67(3):374–378. [PubMed: 14129229]
11. Starr I, et al. Studies on the estimation of cardiac output in man, and of abnormalities in cardiac function, from the heart's recoil and the blood's impacts; the ballistocardiogram. Am J Physiol. Aug; 1939 127(1):1–28.

12. Starr I. Normal standards for amplitude of ballistocardiograms calibrated by force. Circulation. Jun; 1955 11(6):914–926. [PubMed: 14379426]
13. Starr I. Progress towards a physiological cardiology: a second essay on the ballistocardiogram. Ann Intern Med. Dec; 1965 63(6):1079–1105. [PubMed: 5320951]
14. Scarborough WR, et al. Proposals for ballistocardiographic nomenclature and conventions: revised and extended report of committee on ballistocardiographic terminology. Circulation. Sep; 1956 14(3):435–450. [PubMed: 13365056]
15. Corp, NK. Half a century of contributing to medical care and society [Online]. Available: http://www.nihonkohden.com/company/history/1950s.html
16. Elliott RV, et al. Acceleration ballistocardiography design, construction, and application of a new instrument. Circulation. Feb; 1954 9(2):281–291. [PubMed: 13127190]
17. He, D., et al. A continuous, wearable, and wireless heart monitor using head ballistocardiogram (BCG) and head electrocardiogram (ECG). Proc. IEEE Eng. Med. Biol. Soc; Boston, Massachusetts. 2011; p. 4729-4732.
18. Winokur, ES., et al. A wearable vital signs monitor at the ear for continuous heart rate and Pulse Transit Time measurements. Proc. IEEE Eng. Med. Biol. Soc; San Diego, California, USA. 2012; p. 2724-2727.
19. He, D. PhD dissertation. Electrical Engineering, Massachusetts Institute of Technology; Cambridge, Massachusetts, USA: 2013. A wearable heart monitor at the ear using ballistocardiogram (BCG) and electrocardiogram (ECG) with a nanowatt ECG heartbeat detection circuit.
20. Inan OT, et al. Robust ballistocardiogram acquisition for home monitoring. Physiol Meas. Feb; 2009 30(2):169–185. [PubMed: 19147897]
21. Shin JH, et al. Non-constrained monitoring of systolic blood pressure on a weighing scale. Physiol Meas. Jul; 2009 30(7):679–693. [PubMed: 19525570]
22. Shin, JH., et al. HRV analysis and blood pressure monitoring on weighing scale using BCG. Proc. IEEE Eng. Med. Biol. Soc; San Diego, California, USA. 2012; p. 3789-3792.
23. Kim C-S, et al. Ballistocardiogram as proximal timing reference for pulse transit time measurement: potential for cuffless blood pressure monitoring. IEEE Trans Biomed Eng. Nov; 2015 62(11):2657–2664. [PubMed: 26054058]
24. Alametsä, J., et al. The potential of EMFi sensors in heart activity monitoring. Proc. 2nd OpenECG Workshop “Integration of the ECG into the HER & Interoperability of ECG Device Systems”; Berlin, Germany. 2004;
25. Alametsä J, et al. Ballistocardiography in sitting and horizontal positions. Physiol Meas. Aug; 2008 29(29):1071–1087. [PubMed: 18756028]
26. Brüser C, et al. Adaptive beat-to-beat heart rate estimation in ballistocardiograms. IEEE Trans Inf Technol Biomed. Sep; 2011 15(5):778–786. [PubMed: 21421447]
27. Ngai, B., et al. Comparative analysis of seismocardiogram waves with the ultra-low frequency ballistocardiogram. Proc. IEEE Eng. Med. Biol. Soc; Minneapolis, Minnesota, USA. 2009; p. 2851-2854.
28. Krug, JW., et al. Optical ballistocardiography for gating and patient monitoring during MRI: an initial study. Proc. Computing in Cardiology Conference (CinC); Cambridge, Massachusetts. 2014; p. 953-956.
29. Balakrishnan, G., et al. Detecting pulse from head motions in video. Proc. IEEE Computer Vision and Pattern Recognition (CVPR); Portland, Oregon, USA. 2013; p. 3430-3437.
30. Verkruysse W, et al. Remote plethysmographic imaging using ambient light. Opt Exp. Dec; 2008 16(26):21434–21445.
31. de Hann G, et al. Robust pulse rate from chrominance-based rPPG. IEEE Trans Biomed Eng. Oct; 2013 60(10):2878–2886. [PubMed: 23744659]
32. McDuff, D., et al. Remote measurement of cognitive stress via heart rate variability. Proc. IEEE Eng. Med. Biol. Soc; Chicago, Illinois, USA. 2014; p. 2957-2960.
33. Wieringa F, et al. Contactless multiple wavelength photoplethysmographic imaging: a first step toward ‘SpO2 camera’ technology. Ann Biomed Eng. 2005; 33(8):1034–1041. [PubMed: 16133912]

34. Shao D, et al. Noncontact monitoring of blood oxygen saturation using camera and dual-wavelength imaging system. IEEE Trans Biomed Eng. Jun; 2016 63(6):1091–1098. [PubMed: 26415199]
35. Shao D, et al. Noncontact monitoring breathing pattern, exhalation flow rate and pulse transit time. IEEE Trans Biomed Eng. Oct; 2014 61(11):2760–2767. [PubMed: 25330153]
36. Kim CS, et al. Ballistocardiogram as Proximal Timing Reference for Pulse Transit Time Measurement: Potential for Cuffless Blood Pressure Monitoring. IEEE Trans Biomed Eng. Nov; 2015 62(11):2657–2664. [PubMed: 26054058]
37. Gesche H, et al. Continuous blood pressure measurement by using the pulse transit time: comparison to a cuff-based method. Eur J Appl Physiol. Jan; 2012 112(1):309–315. [PubMed: 21556814]
38. Lempe, G., et al. ROI selection for remote photoplethysmography. Proc. Bildverarbeitung für die Medizin; 2013; p. 99-103.
39. Shi, J., et al. Good features to track. Proc. IEEE Computer Vision and Pattern Recognition (CVPR); Seattle, Washington, USA. 1994; p. 593-600.
40. Tomasi, C., et al. Technical Report CMU-CS-91–132. Carnegie Mellon University; Pittsburgh, Pennsylvania, USA: 1991. Detection and tracking of point features.
41. Lucas, B., et al. An Iterative Image Registration Technique with an Application to Stereo Vision. Proc. IJCAI; Vancouver, British Columbia, Canada. 1981; p. 674-679.
42. Wang W, et al. Exploiting spatial redundancy of image sensor for motion robust rppg. IEEE Trans Biomed Eng. Jan; 2015 62(2):415–425. [PubMed: 25216474]
43. Coppola R, et al. Signal to noise ratio and response variability measurements in single trial evoked potentials. Electroencephalogr Clin Neurophysiol. Feb; 1978 44(2):214–222. [PubMed: 75094]
44. Pinheiro E, et al. Theory and developments in an unobtrusive cardiovascular system representation: ballistocardiography. Open Biomed Eng J. Oct.2010 4:201–216. [PubMed: 21673836]
45. Migeotte, P-F., et al. Three dimensional ballistocardiography: methodology and results from microgravity and dry immersion. Proc. IEEE Eng. Med. Biol. Soc; Boston, Massachusetts, USA. 2011; p. 4271-4274.
46. STMicroelectronics. iNEMO inertial module: 3D accelerometer and 3D gyroscope [Online]. Available: www.st.com/resource/en/datasheet/lsm330.pdf
47. Sachdeva S. Fitzpatrick skin typing: applications in dermatology. Indian J Dermatol Venereol Leprol. Jan-Feb;2009 75(1):93–96. [PubMed: 19172048]
48. Henderson Y. The mass-movements of the circulation as shown by a recoil curve. Am J Physiol. Sep.1905 14:287–298.
49. Scarborough WR, et al. The nature of records from ultra-low frequency ballistocardiographic systems and their relation to circulatory events. Am J Cardiol. Nov; 1958 2(5):613–641. [PubMed: 13594849]
50. Burger H, et al. Physical basis of the low-frequency ballistocardiograph. Am Heart J. 1953; 46(1): 71–83. [PubMed: 13057818]
51. Moco A, et al. Ballistocardiographic artifacts in PPG imaging. IEEE Trans Biomed Eng. to be published.
52. Chen, Z., et al. Noninvasive monitoring of blood pressure using optical Ballistocardiography and Photoplethysmograph approaches. Proc. IEEE Eng. Med. Biol. Soc; Osaka, Japan. 2013; p. 2425-2428.
53. Chen, Z., et al. Method and system for optical blood pressure monitoring. US Patent. 20150018637 A1. Jan 15. 2015

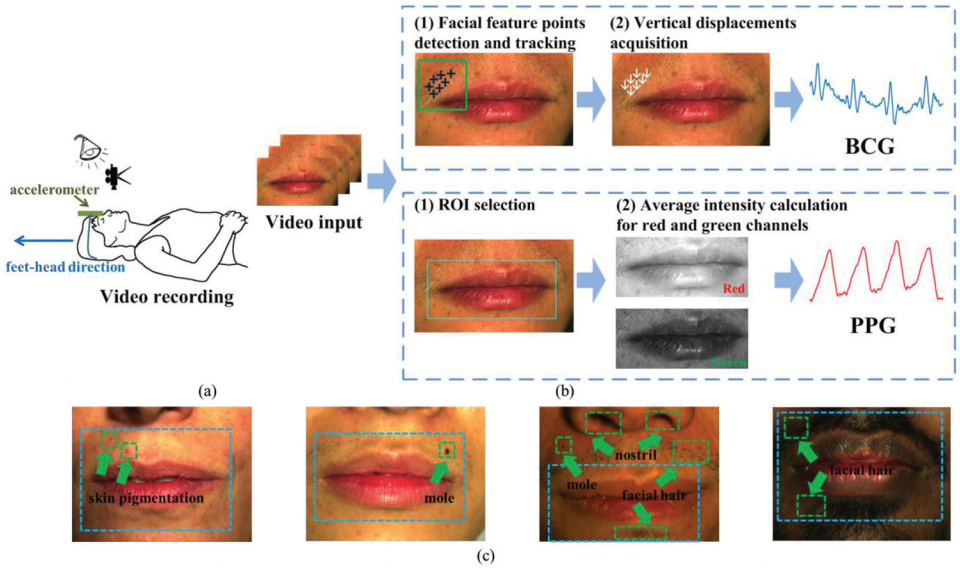

Fig. 1.

Overview of the method. (a) Video recording with reference accelerometer. (b) Flowchart of the presented simultaneous BCG and PPG monitoring method. (c) ROIs and PPG acquisitions. ROIs and related facial features for BCG detection are highlighted in green with arrows. ROIs and PPG detection are highlighted in the blue. Related facial features are annotated in sample images. Estimated skin type from left to right: type II – V.

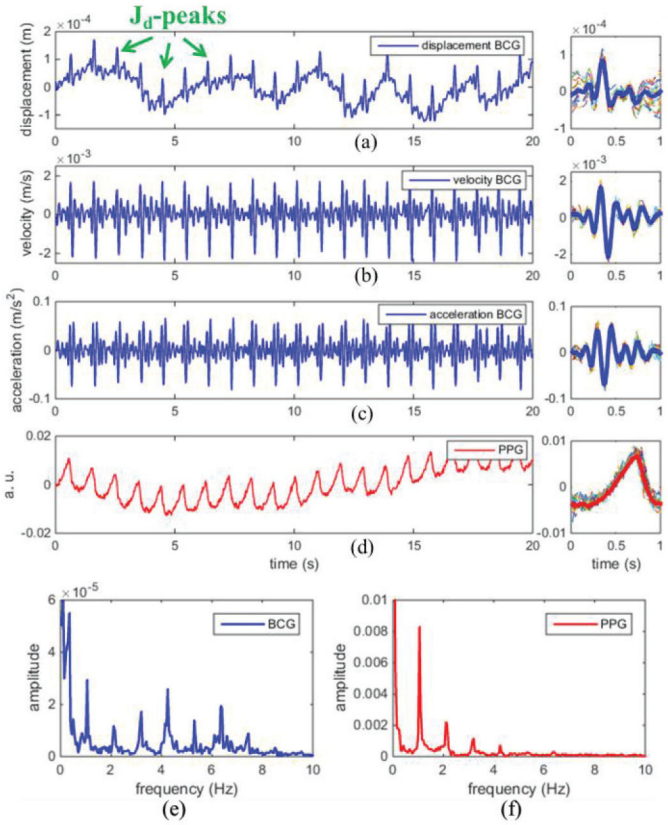

Fig. 2.

(a–d) Detected signals (on the left) with corresponding ensemble averages (on the right). (a) Displacement BCG. (b) Velocity BCG. (c) Acceleration BCG. (d) PPG. (e) Displacement BCG frequency spectrum. (f) PPG frequency spectrum.

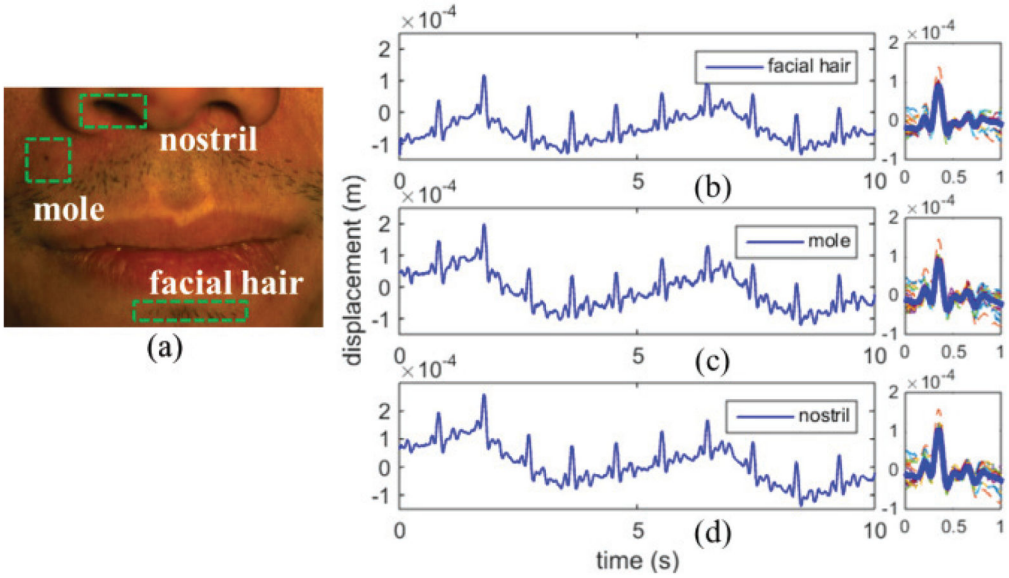

Fig. 3.

BCG waveforms detected from different facial features with corresponding ensemble averages (on the right). (a) Video sample and three different facial features (facial hair, mole and nostril). (b) BCG detected from mole. (c) BCG detected from facial hair. (d) BCG detected from nostril.

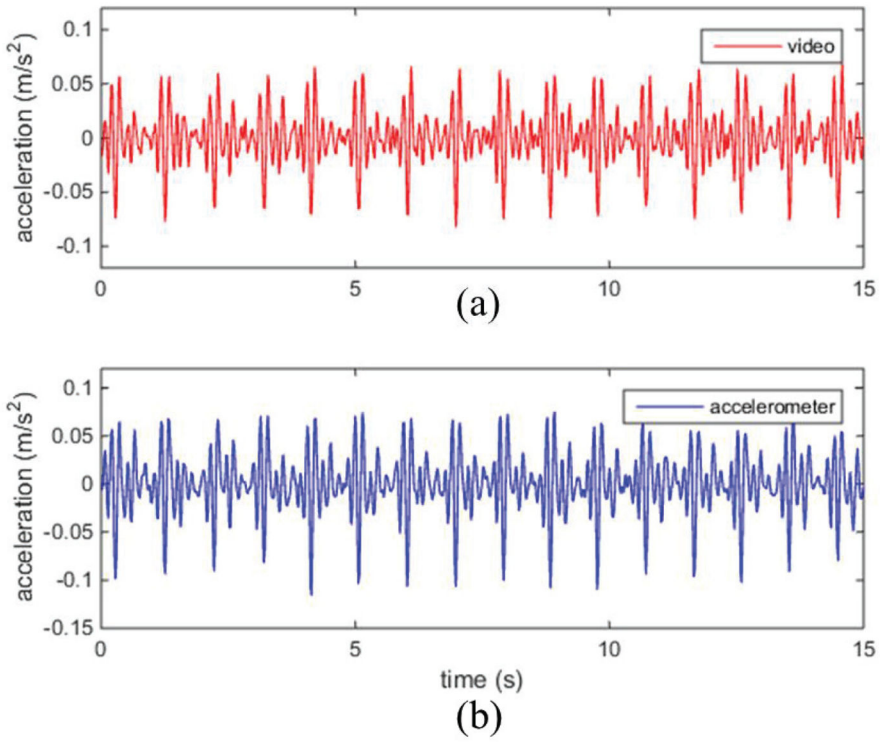

Fig. 4.

BCG validation. (a) Vertical acceleration from video. (b) Vertical acceleration from accelerometer.

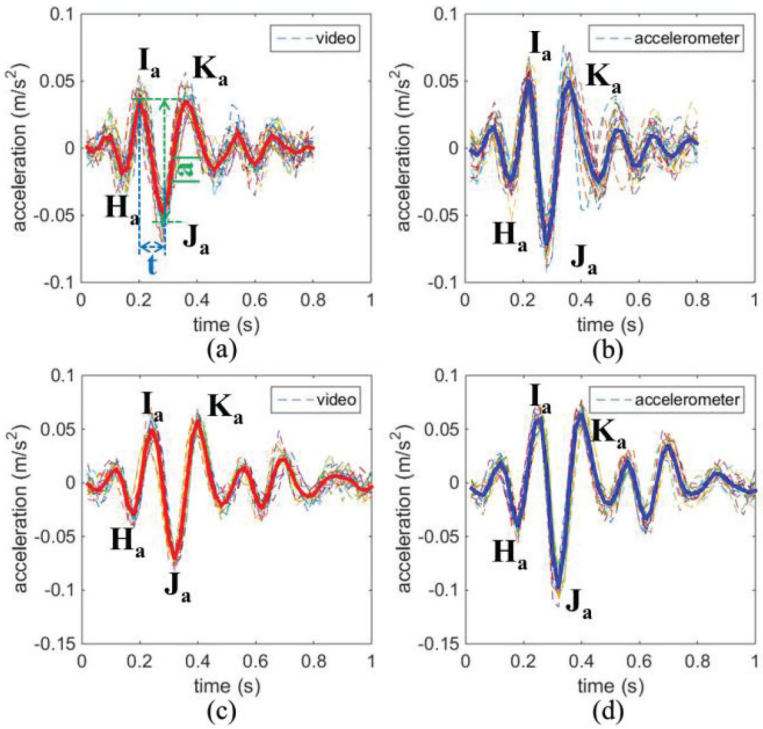

Fig. 5.

Comparison of acceleration BCG waveforms obtained with the presented noncontact method and reference method over 20 seconds. (a) BCG waveforms, for a female subject (heart rate = 1.3 Hz), measured from 25 individual cardiac cycles (dash lines) and ensemble average for the 25 cycles (solid line). The major waves (*H, I, J,* and *K*), IJ amplitude (|*a*|), and IJ interval (*t*) are denoted with letters. (b) BCG for the female subject in (a), measured simultaneously using an accelerometer. (c) BCG waveforms, for a male subject (heart rate = 1.1 Hz), measured from 19 individual cardiac cycles (dash lines) and ensemble average for the 19 cycles (solid line). (d) BCG for the male subject in (c), measured simultaneously using an accelerometer.

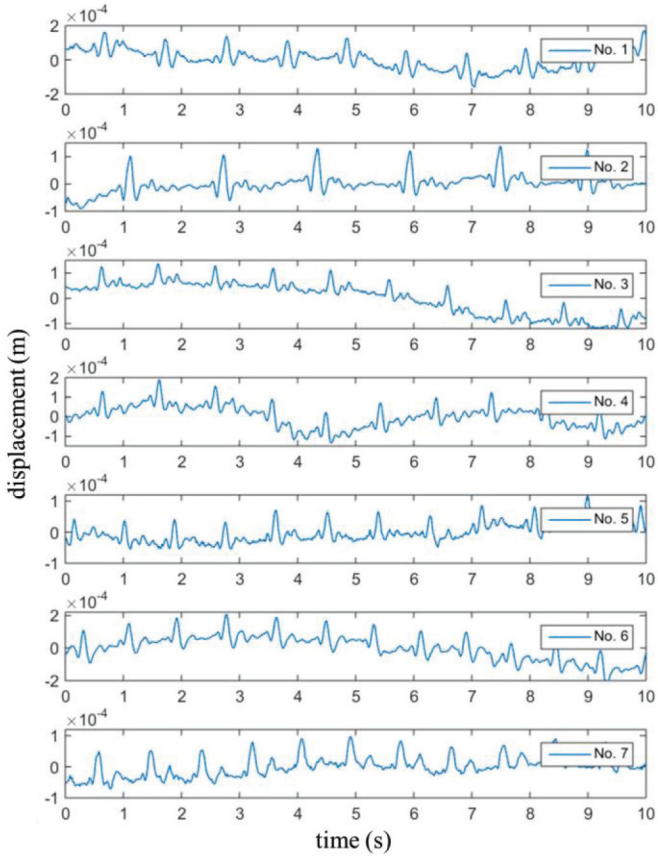

Fig. 6.
Displacement BCGs obtained from different subjects.

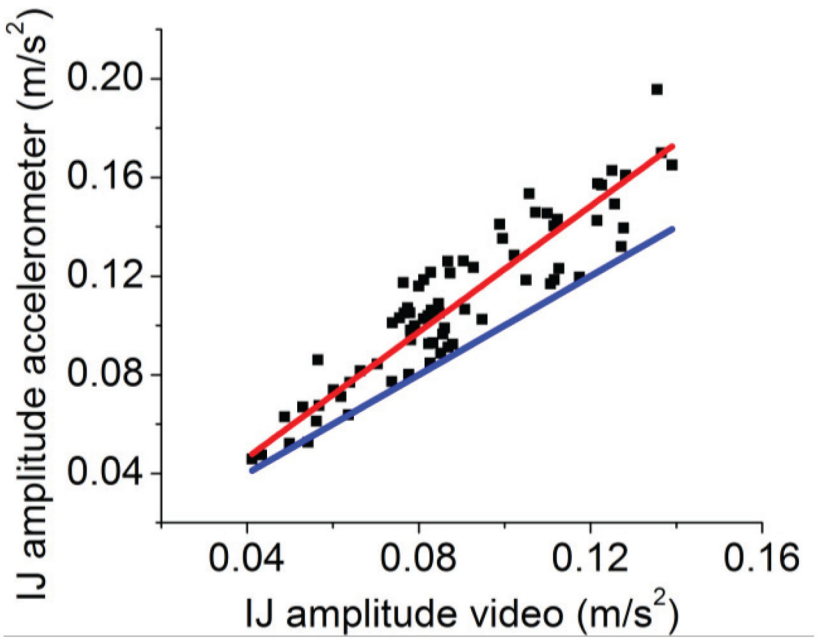

Fig. 7.

Correlation between the IJ amplitudes of acceleration BCGs obtained using the presented and reference methods. The red line is a linear fit of the scattered data. The blue line is the identity line (slope = 1).

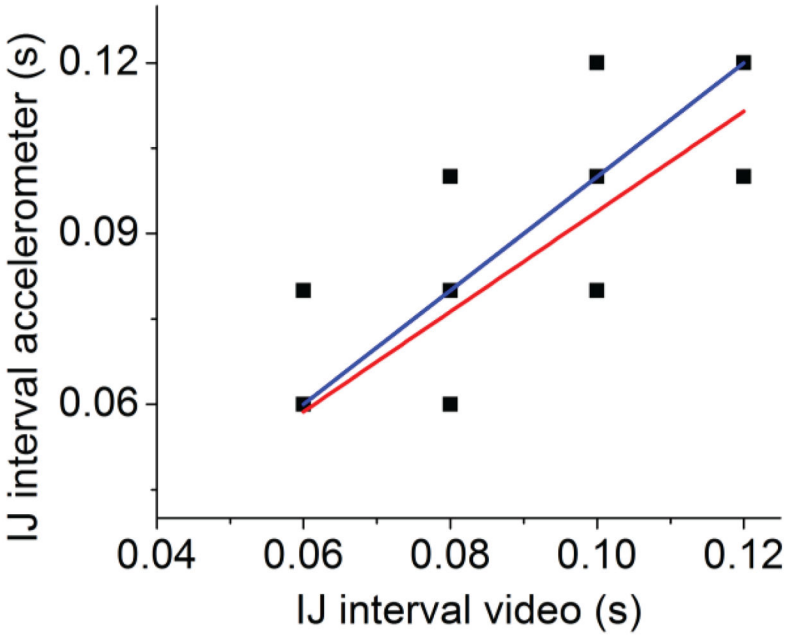

Fig. 8.

Correlation between the IJ intervals of acceleration BCGs obtained using the presented and reference methods. The red line is a linear fit of the scattered data. The blue line is the identity line (slope = 1). The plot has overlapping data points.

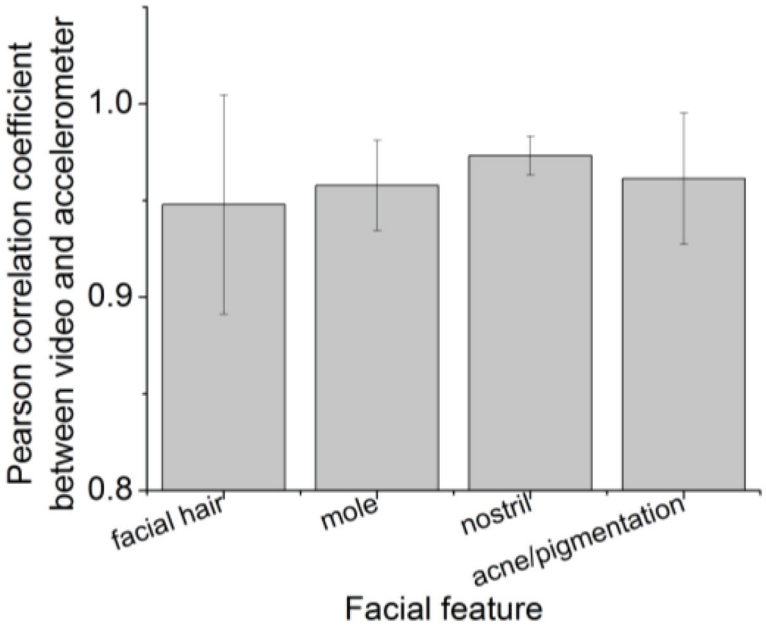

Fig. 9.

Pearson correlation coefficients between the presented method and accelerometer, with standard deviation, based on different facial features.

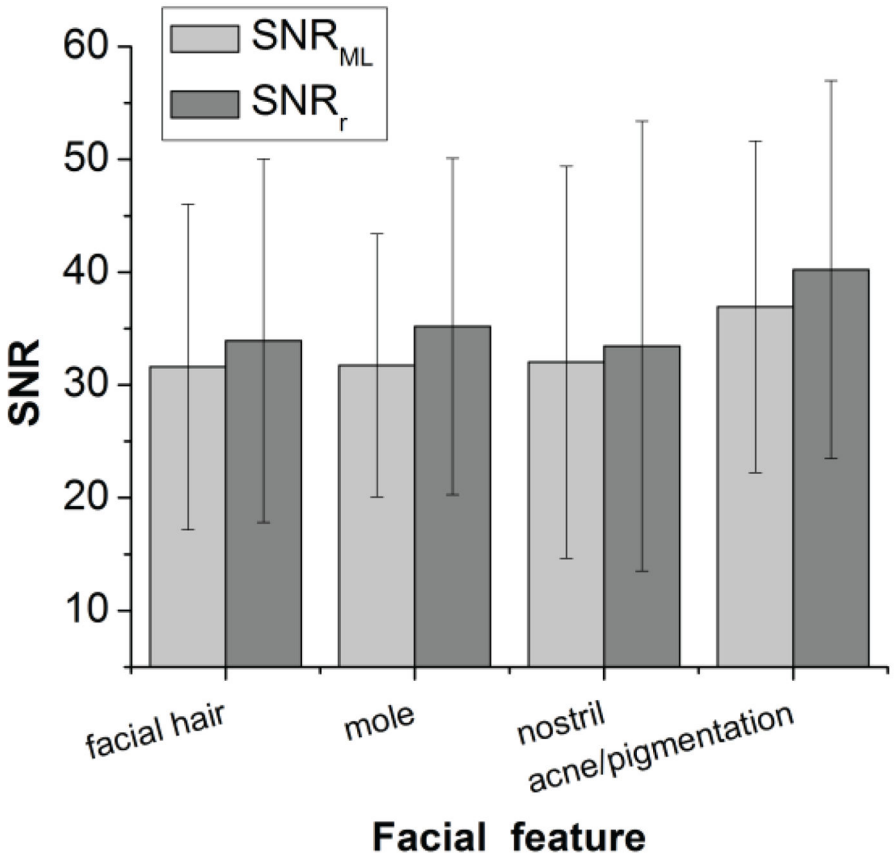

Fig. 10.

SNR estimation of BCG using the presented method, with standard deviation, based on maximum likelihood (SNR_{ML}) and sample correlation coefficient (SNR_r).

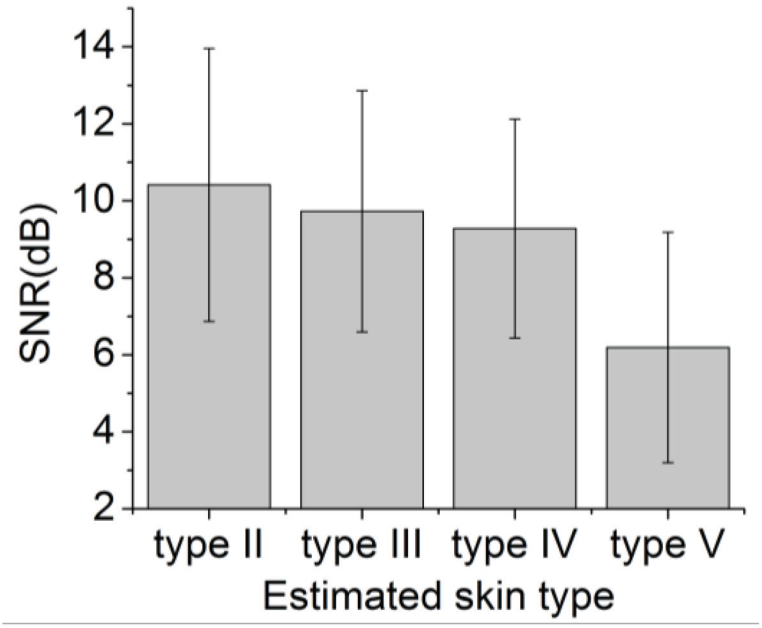

Fig. 11.
SNR of PPG from different skin categories with standard deviation.

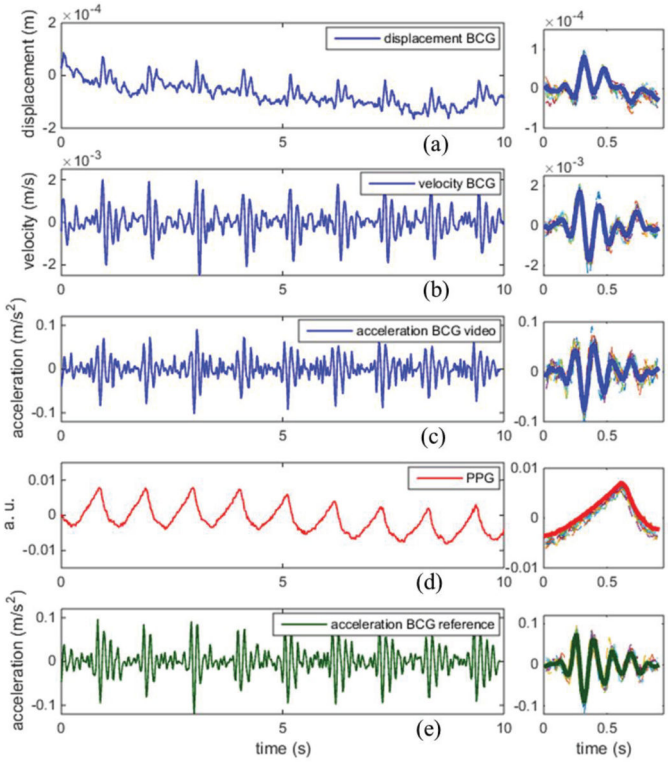

Fig. 12.

(a–e) Detected signals (on the left) with corresponding ensemble averages (on the right). (a) Displacement BCG. (b) Velocity BCG. (c) Acceleration BCG from video-based method. (d) PPG. (e) Acceleration BCG from reference device.

TABLE I

BCG VALUES COMPARISON

BCG Type	References	Presented Method
displacement (m)	6×10^{-5} [28], 1.5×10^{-4} [50], 10^{-4} [45]	1.5×10^{-4}
velocity (m/s)	2.5×10^{-3} [28]	4×10^{-3}
acceleration (m/s^2)	0.1 [9, 17], 0.08 [45]	0.009

The reference values are estimated from the reported test results (plots). The values from the presented method are averaged over 23 healthy subjects.